Contact Ion Pairs. Picosecond Dynamics of Solvent Separation, Internal Return, and Special Salt Effect

T. Yabe and J. K. Kochi*

Contribution from the Chemistry Department, University of Houston, Houston, Texas 77204-5641. *Received December 9, 1991*

Abstract: Direct observation by time-resolved picosecond spectroscopy of the contact ion pair (CIP) allows the microdynamical rate constants for its (a) annihilation by internal return, (b) relaxation to the solvent-separated ion pair (SSIP), and (c) ionic exchange in the special salt effect to be quantitatively evaluated for the solvolysis mechanism (Scheme I) originally formulated by Winstein and co-workers. The relevant contact ion pair [Ar^+,T^-] is spontaneously generated by the 20-ps laser pulse excitation of the EDA complex from tetranitromethane (TNO_2) and anthracene (Ar). The use of a series of 9-Y-anthracenes with graded substituents (Y = nitro > cyano > formyl > bromo > hydrogen > vinyl > methyl) provides the structurally related cations (Ar^+) possessing diagnostic absorption bands and of significantly differing reactivities to modulate ion-pair dynamics. The temporal relaxation of each CIP follows uniquely from the time-resolved spectroscopy of Ar^+. The varied (picosecond) decay patterns of the cation absorbance are characterized by first-order kinetics (k_{obsd}) to limiting residuals (R)—all in solvents varying from acetonitrile (polar), chloroform, dichloromethane, benzene, to *n*-hexane (nonpolar). The rigorous dissection of k_{obsd} and R for the contact ion pair in Scheme I yields the individual rate constants for internal return (k_1) and solvent separation into SSIP (k_2). The variation in ion-pair microdynamics (k_1, k_2) with changes in cation reactivity (given by the Hammett substituent parameter for Y) and solvent polarity (taken as the Kosower Z-value) is discussed in terms of CIP structure and the driving force for internal return. The interception of the contact ion pair by added salt is measured by the second-order rate constant (k_x) for ion-pair exchange (eq 15). The time constant for k_x[salt] identifies the temporal operation of the special salt effect on the contact ion pair to be as short as 10 ns at salt concentrations as low as 5×10^{-3} M. Ion-pair reversibility CIP $\rightleftharpoons$ SSIP is exergonic by $\sim$2 kcal mol^{-1} in dichloromethane, and thus external ion-pair return (k_{-2}) is shown to be too slow to affect the picosecond dynamics of the contact ion pair.

Introduction

Reactive ions and ion pairs are intrinsic to a variety of reaction mechanisms in solution,[1-3] but their dynamic behavior is largely deduced from solvent-assisted substitutions of organic derivatives (RX).[4] The critical examination and elegant analysis of solvolysis kinetics have led to Winstein's formulation[5] of (a) internal return of the initially-formed contact (intimate) ion pairs (CIP) in competition with (b) their separation into solvent-separated (loose) ion pairs (SSIP) that occurs prior to the diffusional processes leading to the free ions, as summarized in Scheme I.[6] The complex kinetics associated with Scheme I is further complicated by (c) the special salt effect arising from the interception of the contact ion pair by salt that is commonly added to maintain constant ionic strength.[7] As a result, the general (analytical) solutions to the rate expressions have merely yielded rate ratios,[8] but not the requisite individual rate constants for ascertaining the effects of structural changes of R and X on the various ion-pair dynamics—especially as they are modulated by solvent polarity and added salt.[9]

Scheme I

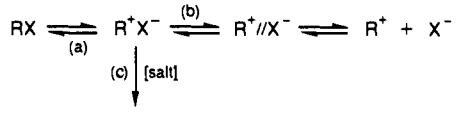

Since the heterolysis of the R–X bond is the rate-limiting (activation) process in S_N1 solvolysis, an alternative (nonadiabatic) methodology is clearly required to generate the contact ion pair (CIP) in sufficient concentrations to directly observe its temporal evolution, viz., internal return,[10] separation to SSIP,[11] special salt effect,[12] etc. Indeed, laser flash photolytic techniques[13] offer the experimental means to spontaneously produce contact ion pairs by various photoinduced electron-transfer processes between uncharged electron donors (D) and acceptors (A).[14-17] However,

(1) Szwarc, M., Ed. *Ions and Ion Pairs in Organic Reactions*; Wiley: New York, 1972, 1974; Vols. 1 and 2.
(2) Gordon, J. E. *Organic Chemistry of Electrolyte Solutions*; Wiley: New York, 1975.
(3) Lowry, T. H.; Richardson, K. H. *Mechanism and Theory in Organic Chemistry*, 3rd ed.; Harper & Row: New York, 1985.
(4) Ingold, C. K. *Structure and Mechanism in Organic Chemistry*; Cornell University Press: Ithaca, NY, 1969.
(5) (a) Winstein, S.; Klinedinst, P. E., Jr.; Robinson, G. C. *J. Am. Chem. Soc.* **1961**, *83*, 885. (b) Winstein, S.; Klinedinst, P. E., Jr.; Clippinger, E. *J. Am. Chem. Soc.* **1961**, *83*, 4986. (c) Winstein, S.; Robinson, G. C. *J. Am. Chem. Soc.* **1958**, *80*, 169 and related papers.
(6) For reviews, see: (a) Harris, J. M. *Prog. Phys. Org. Chem.* **1974**, *11*, 89. (b) Reference 1, Vol. 2, Chapter 3, p 247 ff. (c) Shiner, V. J., Jr. In *Isotope Effects in Chemical Reactions*; Collins, C. J., Bowman, N. W., Eds.; Van Nostrand Reinhold: New York, 1970.
(7) (a) The "special" salt effect is used here interchangeably with ion-pair exchange and in this general context is to be distinguished from the "normal" salt effect.[1,2] As originally conceived by Winstein and co-workers,[12] the special salt effect was phenomenological and thus applied (rather restrictedly) to the relatively slow processes[2,7] involving the SSIP. (b) For early suggestions relating to ion-pair exchange of CIP, see: Sneen, R. A. *Acc. Chem. Res.* **1973**, *6*, 46.
(8) See, for example: Winstein, S.; Clippinger, E.; Fainberg, A. H.; Heck, R.; Robinson, G. C. *J. Am. Chem. Soc.* **1956**, *78*, 328.
(9) Reichardt, C. *Solvent and Solvent Effects in Organic Chemistry*, 2nd ed.; VCH: Weinheim, Germany, 1988.
(10) (a) Young, W. G.; Winstein, S.; Goering, H. L. *J. Am. Chem. Soc.* **1951**, *73*, 1958. (b) Winstein, S.; Trifan, D. *J. Am. Chem. Soc.* **1952**, *74*, 1154. (c) Winstein, S.; Schreiber, K. C. *J. Am. Chem. Soc.* **1952**, *74*, 2165. (d) Paradisi, C.; Bunnett, J. F. *J. Am. Chem. Soc.* **1985**, *107*, 8223. Compare also: Ritchie, C. D. *Pure Appl. Chem.* **1979**, *51*, 153, **1978**, *50*, 1281. Kessler, H.; Feigel, M. *Acc. Chem. Res.* **1982**, *15*, 2.
(11) (a) Winstein, S.; Clippinger, E.; Fainberg, A. H.; Robinson, G. C. *J. Am. Chem. Soc.* **1954**, *76*, 2597. (b) Sadek, H.; Fuoss, R. M. *J. Am. Chem. Soc.* **1954**, *76*, 5905.
(12) Fainberg, A. H.; Winstein, S. *J. Am. Chem. Soc.* **1956**, *78*, 2763, 2767.
(13) For example, see: Barbara, P. F.; Brus, L. F.; Rentzepis, P. M. *Chem. Phys. Lett.* **1980**, *64*, 447. Hochstrasser, R. P. *Pure Appl. Chem.* **1982**, *52*, 2683. Wang, Y.; Crawford, M. C.; Eisenthal, K. B. *J. Phys. Chem.* **1980**, *84*, 2696.
(14) (a) Simon, J. D.; Peters, K. S. *Acc. Chem. Res.* **1984**, *17*, 277. (b) Goodman, J. L.; Peters, K. S. *J. Am. Chem. Soc.* **1985**, *107*, 6459; **1986**, *108*, 1700. (c) Schaefer, C. G.; Peters, K. S. *J. Am. Chem. Soc.* **1980**, *102*, 7566. (d) Simon, J. D.; Peters, K. S. *J. Am. Chem. Soc.* **1981**, *103*, 6403. (e) Simon, J. D.; Peters, K. S. *J. Am. Chem. Soc.* **1982**, *104*, 6542; **1983**, *105*, 4875.
(15) (a) Mataga, N. *Pure Appl. Chem.* **1984**, *56*, 1255. (b) Masuhara, H.; Mataga, N. *Acc. Chem. Res.* **1981**, *14*, 312. (c) Mataga, N.; Kanda, Y.; Okada, T. *J. Phys. Chem.* **1986**, *90*, 3880. (d) Ojima, S.; Miyasaka, H.; Mataga, N. *J. Phys. Chem.* **1990**, *94*, 5834. (e) Ojima, S.; Miyasaka, H.; Mataga, N. *J. Phys. Chem.* **1990**, *94*, 7534 and references therein.
(16) (a) Weller, A. *Z. Phys. Chem.* **1982**, *133*, 93. (b) Beens, H.; Weller, A. In *Organic Molecular Photophysics*; Birks, J. B., Ed.; Wiley: New York, 1975; Vol. 2, p 159. (c) Gould, I. R.; Moody, R.; Farid, S. *J. Am. Chem. Soc.* **1988**, *110*, 7242. (d) Gould, I. R.; Ege, D.; Moser, J. E.; Farid, S. *J. Am. Chem. Soc.* **1990**, *112*, 4290.
(17) Fox, M. A., Chanon, M., Eds. *Photoinduced Electron Transfer*; Elsevier: New York, 1988; Part C.

0002-7863/92/1514-4491$03.00/0

Table I. Absorption Spectra of Transient Cations in Different Solvents

Ar^+ Y^a	MeCN λ (fwhm)[b]	CH_2Cl_2 λ (fwhm)[b]	$CHCl_3$ λ (fwhm)[b]	C_6H_6 λ (fwhm)[b]	n-C_6H_{14} λ (fwhm)[b]
nitro (N^+)	755 (12)	760 (14)	755 (11)	755 (12)	[c]
cyano (C^+)	760 (12)	770 (16)	760 (10)	765 (10)	[c]
formyl (F^+)	755 (11)	755 (14)	755 (14)	765 (17)	740 (7)
bromo (B^+)	710 (11)	710 (10)	710 (11)	730 (19)	710 (18)
hydrogen (H^+)	725 (11)	725 (9)	725 (11)	745 (14)	725 (10)
vinyl (V^+)	710 (12)	700 (11)	700 (19)	710 (22)	700 (18)
methyl (M^+)	685 (11)	695 (12)	695 (11)	715 (10)	695 (14)

[a] Substituent at the 9-position of the anthracene donor. [b] Absorption maximum in nm (±5 nm) and $\Delta\nu$ (bandwidth) in 10^2 cm^{-1} (±10%) in parentheses. [c] Not measured.

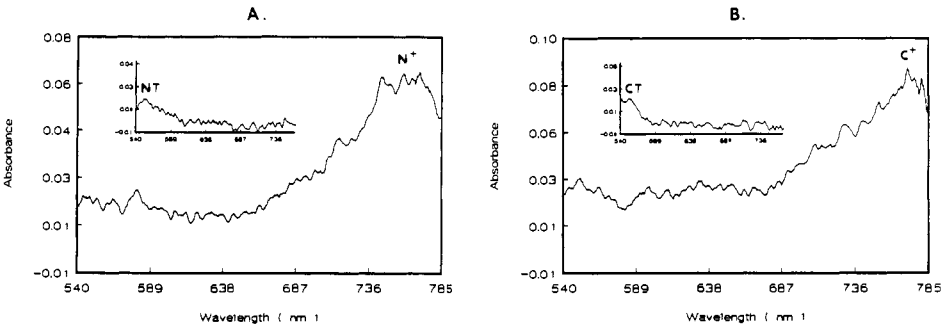

Figure 1. Spontaneous appearance of the cations N^+ and C^+ at 0 ps upon the 532-nm excitation of the EDA complex from tetranitromethane with 9-nitroanthracene (left) and 9-cyanoanthracene (right) in dichloromethane with a 20-ps (fwhm) laser pulse. The inset is the residual absorption spectrum after 2.6 ns, showing the growth of the covalent adduct ArT at $\lambda_{max} \approx 550$ nm and the complete decay of N^+ and C^+.

owing to the possible structural ambiguity (e.g., distortion, separation, spin state, partial binding, etc.) in this paramagnetic type of radical ion pair ($D^{\bullet+}$, $A^{\bullet-}$),[18] we have focused our attention on the transient CIP in which at least one component is a diamagnetic ion.[19,20] Thus we previously showed that various aromatic donors (Ar) form a series of weak 1:1 complexes with tetranitromethane (TNO_2),[22]

$$Ar + TNO_2 \overset{K_{EDA}}{\rightleftharpoons} [Ar,TNO_2] \quad (1)$$

which exhibit characteristic charge-transfer (CT) absorption bands associated with electron donor–acceptor or EDA interactions of the type originally described by Mulliken.[23] Most importantly, the specific irradiation of the CT band resulted in electron transfer to produce simultaneously the aromatic cation (Ar^+) and trinitromethide anion (T^-) in the ground state,[24]

$$[Ar,TNO_2] \xrightarrow[(<10\ ps)]{h\nu_{CT}} [Ar^+,T^-]NO_2 \quad (2)$$

within ~10 ps, i.e, the rise time of the laser pulse.[22] Since this time scale effectively minimizes competition from diffusional processes,[25] the *cation and anion are born as a contact ion pair* initially trapped within the solvent cage (brackets in eq 2), with an interionic distance that is equivalent to the intermolecular separation extant in the inner-sphere EDA precursor.[26] Photochemical and product studies with different aromatic donors have established the final photoadduct to be subsequently formed with high quantum yields via the efficient (re)combination of the fragments from eq 2 by two sequential chemical reactions, namely,[27]

$$[Ar^+,T^-]NO_2 \rightarrow ArT + NO_2 \quad (3)$$

$$ArT + NO_2 \rightarrow ArT(NO_2) \quad (4)$$

The first step is tantamount to CIP annihilation, and it corresponds to internal return in solvolysis.[28] Accordingly, we describe in this study the solvent and salt effects on the picosecond dynamics accompanying (a) the annihilation (internal return) of the contact ion pair $[Ar^+,T^-]$ to form the covalent adduct ArT in competition with (b) its relaxation to the solvent-separated ion pair $Ar^+//T^-$ in order to quantitatively evaluate the individual rate constants pertinent to the initial phases of the ion-pair dynamics, as outlined in Scheme I.

(18) (a) Simon, J. D.; Peters, K. S. *J. Am. Chem. Soc.* **1983**, *105*, 4875. (b) Devadoss, C.; Fessenden, R. W. *J. Phys. Chem.* **1990**, *94*, 4540. (c) Wasielewski, M. R. In *Photoinduced Electron Transfer*; Fox, M. A., Chanon, M., Eds.; Elsevier: New York, 1988; Part A, p 161. Wilkinson, F. In ref 18c, p 207. (d) Nagakura, S. In *Excited States*; Lim, E. C., Ed.; Academic: New York, 1975; Vol. 2, pp 321 ff. (e) Schnapp, K. A.; Wilson, R. M.; Ho, D. M.; Caldwell, R. A.; Creed, D. *J. Am. Chem. Soc.* **1990**, *112*, 3700. (f) Asahi, T.; Mataga, N. *J. Phys. Chem.* **1989**, *93*, 6575. (g) Bockman, T. M.; Karpinski, Z.; Sankararaman, S.; Kochi, J. K. *J. Am. Chem. Soc.* **1992**, *114*, 1970.

(19) For a preliminary report, see: Yabe, T.; Sankararaman, S.; Kochi, J. K. *J. Phys. Chem.* **1991**, *95*, 4177.

(20) The spontaneous generation of diamagnetic ClPs by flash photolysis of solvolytic systems[21] may be suitable in nanosecond time resolution, but extraneous excited states and byproducts[21c] may complicate the picosecond studies of relevance here.

(21) (a) McClelland, R. A.; Kanagasabapathy, V. M.; Banait, N. S.; Steenken, S. *J. Am. Chem. Soc.* **1989**, *111*, 3966; **1991**, *113*, 1009. (b) Kobayashi, S.; Zhu, Q. Q.; Schnabel, W. *Z. Naturforsch.* **1988**, *436*, 825. (c) Cristol, S. J.; Stull, D. P.; McEntee, T. E. *J. Org. Chem.* **1978**, *43*, 1756 and references therein. (d) Spears, K. G.; Gray, T. H.; Huang, D.-Y. *J. Phys. Chem.* **1986**, *90*, 779. See also: Manring, L. E.; Peters, K. S. *J. Phys. Chem.* **1984**, *88*, 315. Jones, G., II; Goswani, K. *J. Phys. Chem.* **1986**, *90*, 5414.

(22) Masnovi, J. M.; Hilinski, E. F.; Rentzepis, P. M.; Kochi, J. K. *J. Am. Chem. Soc.* **1986**, *108*, 1126.

(23) Mulliken, R. S. *J. Am. Chem. Soc.* **1952**, *74*, 811. Mulliken, R. S.; Person, W. B. *Molecular Complexes*; Wiley: New York, 1969.

(24) Hereinafter, the electron (dot) is omitted from the aromatic cation radical (Ar^+) and the covalent adduct (ArT).

(25) The time resolution of <3 ps is limited by the dissociative electron attachment to TNO_2. See: Chaudhuri, S. A.; Asmus, K. D. *J. Phys. Chem.* **1972**, *76*, 26 and Masnovi et al. in ref 22.

(26) For the intermolecular separations in weak EDA (inner-sphere) complexes, see: (a) Herbstein, F. H. In *Perspectives in Structural Chemistry*; Dunitz, J. D., Ibers, J. A., Eds.; Wiley: New York, 1971; Vol. 4, pp 166 ff. (b) Prout, C. K.; Kamenar, B. *Mol. Complexes* **1973**, *1*, 152. (c) Soos, Z. G.; Klein, D. J. *Mol. Assoc.* **1975**, *1*, 2. (d) Takahashi, Y.; Sankararaman, S.; Kochi, J. K. *J. Am. Chem. Soc.* **1989**, *111*, 2954.

(27) (a) Masnovi, J. M.; Kochi, J. K. *J. Am. Chem. Soc.* **1985**, *107*, 7880. (b) Masnovi, J. M.; Kochi, J. K. *J. Org. Chem.* **1985**, *50*, 5245.

(28) (a) The covalent adduct ArT has the hydranthryl structure:

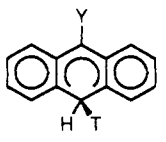

(b) The kinetics of the second step (eq 4) involving uncharged species was presented in ref 27a.

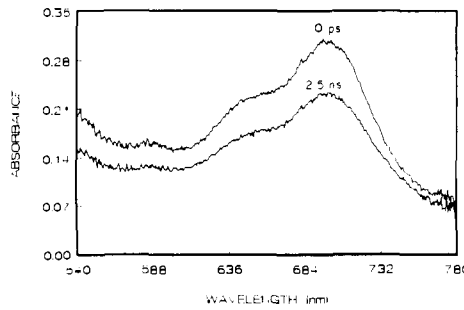

Figure 2. Temporal evolution of the absorption spectrum of V^+ taken at 0 ps and 2.5 ns after the 532-nm excitation of $[V,TNO_2]$ in chloroform with a 20-ps (fwhm) laser pulse.

Results

The desirable series of reactive cations for this study should consist of related ionic structures with roughly the same (large) size, but of significantly differing reactivities. As such, we considered the aromatic donor of choice to be anthracene and its derivatives owing to the b_{2g} symmetry of the HOMO to afford cations with maximum charge density localized at the two central (meso) positions.[29] The anthracene cation (H^+) and its 9-Y-substituted derivatives with Y = nitro (N^+), cyano (C^+), vinyl (V^+), formyl (F^+), bromo (B^+), and methyl (M^+) were spontaneously generated as follows.

I. Time-Resolved Picosecond Spectroscopy of Charge-Transfer Excitation of the Anthracene EDA Complexes with Tetranitromethane. When an equimolar solution of anthracene (0.1 M) and tetranitromethahe in dichloromethane was irradiated at 532 nm,[30] a new absorption band centered at λ_{max} 725 nm was immediately observed, i.e., within the 20-ps (fwhm) laser pulse. Spectral comparison with the absorption spectrum of anthracene cation generated independently by a spectroelectrochemical technique[31] established the identity of H^+. Similar absorption bands are observed with the 9-substituted anthracene derivatives, and the corresponding cations are identified in Table I, together with the associated values of λ_{max} and bandwidths ($\Delta\nu$) in various solvents. Although the spectral window of 400–800 nm (allowed by the white light continuum[32]) did not permit the simultaneous observation of the trinitromethide anion with λ_{max} 350 nm, the related (nanosecond) studies[27,33] previously showed that the cation/anion pairs Ar^+ and T^- were always cogenerated according to the stoichiometry in eq 2.

The transient character of the new absorption bands was shown by the complete decay of the absorbance back to the base line within 2.6 ns, as illustrated in Figure 1 for the nitro and cyano derivatives N^+ and C^+, respectively, in dichloromethane. The methyl analogue M^+ was largely undiminished within the same time span, and the vinyl-substituted cation V^+ showed intermediate behavior under the same conditions. For the latter, Figure 2 typically illustrates the absence of a band shift or change in band shape accompanying the spectral evolution of the aromatic cation in the time span between 0 ps and 2.6 ns.[34] Moreover, the same absorption spectra of all anthracene cations were observed in the presence of an inert salt that was added as tetra-*n*-butylammonium perchlorate (TBA^+P^-) to solutions in benzene, chloroform, dichloromethane, and acetonitrile.

The spectral decays of the highly transient cations N^+ and C^+ with nitro and cyano substituents in Figure 1 showed residual absorbances centered at λ_{max} ~550 nm that were readily revealed in the 2.6-ns spectra (see insets). Moreover, the monotonic increase in the absorbance of the 550-nm band that accompanied the spectral decay of the related cation F^+, as illustrated by the isosbestic point in Figure 3B at the intermediate time intervals of 150, 300, 700, and 1200 ps, was readily assigned to the concomitant chemical change corresponding to the ion-pair annihilation to the covalent adduct:

$$Ar^+ + T^- \rightarrow ArT \qquad (5)$$

Table II lists the consistent set of extinction coefficients of ArT evaluated at various time intervals on the basis of the measured extinction coefficients of the anthracene cations[35] and the 1:1 stoichiometry in eq 5. Further support for this spectral assignment is obtained by comparison of the spectral maximum (λ_{max}) and extinction coefficient (ϵ_{max}) with those of structurally related species.[36-38]

II. Decay Kinetics of the Transient Cations. The spectral decays of the cation absorbances of N^+ and C^+ in Figure 1 were initially monitored at λ_{mon} 770 nm to correspond with the maximum or near maximum of the absorption bands (Table I). The fitting of the picosecond absorbance (Abs) data was based on the nonlinear least-squares program utilizing the Gauss–Newton algorithm,[39] as described in the Experimental Section. The first-order kinetics of the return (completely to the base line) is illustrated in Figure 4 by the fit of the smooth (decay) lines to the experi-

Table II. Absorbances of the Covalent Adducts[a]

	temporal evolution (ps)[c]					
ArT adduct Y[b]	50	200	450	1000	2000	$\bar{\epsilon}$[d]
nitro (NT)	21	20	26	26	22	2300
cyano (CT)	22	25	20	23	24	2200
formyl (FT)[e]	73	91	82	85	89	8400

[a] Obtained by spectral subtraction at λ 550 nm in dichloromethane, unless indicated otherwise. [b] Substituent at the 9-position of the anthracene donor. [c] Extinction coefficient of the covalent adducts in 10^2 M^{-1} cm^{-1}, as described in the Experimental Section. [d] Extinction coefficient (average) in M^{-1} cm^{-1} (±20%). [e] In benzene.

Table III. Picosecond Decays and (2.5-ns) Residuals of Various Cations[a]

Ar^+ 9-Y-anthracene	$E_{ox}°$ (V vs SCE)[b]	$k_{obsd}(Ar^+)$ (10^9 s^{-1})[c]	R[d]	$k_{obsd}(ArT)$ (10^9 s^{-1})[e]
nitro (N^+)	1.83	3.6	0	4[f]
cyano (C^+)	1.78	3.1	0	3[f]
formyl (F^+)	1.70	2.8	0.25	e[f,g]
bromo (B^+)	1.45	1.6	0.50	h
hydrogen (H^+)	1.49	1.8	0.48	h
vinyl (V^+)	~1.3	1.5	0.60	h
methyl (M^+)	1.26	1.2	0.75	h

[a] Following the 532-nm excitation of $[Ar,TNO_2]$ in dichloromethane solution at 23 °C with a 20-ps laser pulse. [b] Oxidation potential from ref 31. [c] Decay rate (±5%). [d] See text for the definition of the residual fraction. [e] Growth rate (±30%). [f] From the growth of the 550-nm absorption band. [g] Initial (~50%) portion. [h] Not observed.

(29) Klasinc, L.; Kovac, B.; Gusten, H. *Pure Appl. Chem.* **1983**, *55*, 289.
(30) This excitation wavelength (λ_{exc}) is included in the charge-transfer absorption bands (λ_{CT}) of all of the anthracene EDA complexes with tetranitromethane.[27] Since none of the anthracenes and tetranitromethane absorb in this region, only the EDA complex was unambiguously excited according to eq 2.[22]
(31) Masnovi, J. M.; Seddon, E. A.; Kochi, J. K. *Can. J. Chem.* **1984**, *62*, 2552. See also: Torikai, A.; Kato, R. *J. Polym. Sci., Polym. Chem.* **1978**, *16*, 1487.
(32) Hubig, S. M.; Rodgers, M. A. J. In *Handbook of Organic Photochemistry*; Scaiano, J. C., Ed.; CRC Press: Boca Raton, FL, 1989; Vol. 1, p 319.
(33) (a) Masnovi, J. M.; Sankararaman, S.; Kochi, J. K. *J. Am. Chem. Soc.* **1989**, *111*, 2263. (b) Sankararaman, S.; Haney, W. A.; Kochi, J. K. *J. Am. Chem. Soc.* **1987**, *109*, 7824. See also refs 23 and 27.
(34) Thus the spectral shift in the anthracene system is, by itself, insufficient to distinguish the contact ion pair from solvent-separated ion pairs and free ions (compare Figure 2). For spectral shifts in other ion pairs, see ref 14.
(35) The extinction coefficients of C^+, N^+, and F^+ were taken as 11 000, 9900, and 9000 M^{-1} cm^{-1} ±10% [Bockman, T. M. Unpublished results]. Compare: Wang, Y.; Tria, J. J.; Dorfman, L. M. *J. Phys. Chem.* **1979**, *83*, 1946.
(36) See: Okada, T.; Kida, K.; Mataga, N. *Chem. Phys. Lett.* **1982**, *88*, 157 for α-cyanobenzhydryl radical (λ_{max} ≈ 530 nm).
(37) Shida, T. *Electronic Absorption Spectra of Radical Ions*; Elsevier: Amsterdam, 1988. See Figure 15, p 17 for α-hydroxybenzhydryl radical λ_{max} ≈ 560 nm (ϵ, 4×10^3 M^{-1} cm^{-1}).
(38) Bromberg, A.; Schmidt, K. H.; Meisel, D. *J. Am. Chem. Soc.* **1985**, *107*, 83.
(39) Jacobs, D. *The State of the Art in Numerical Analysis*; Academic: New York, 1976.

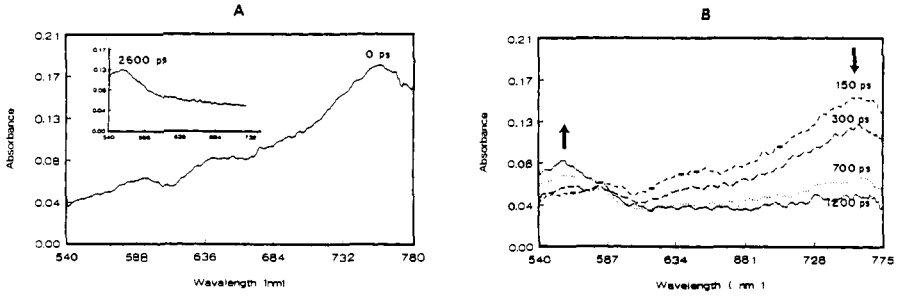

Figure 3. Simultaneous growth of the covalent adduct FT (with λ_{max} 550 nm) and decay of the cation F^+ (λ_{max} 755 nm) as shown by the changes in the time-resolved absorption spectrum taken at (A) 0 ps (inset at 2.6 ns) and (B) intermediate intervals of 150, 300, 700, and 1200 ps (as indicated), following the application of a 20-ps laser pulse to the EDA complex in dichloromethane.

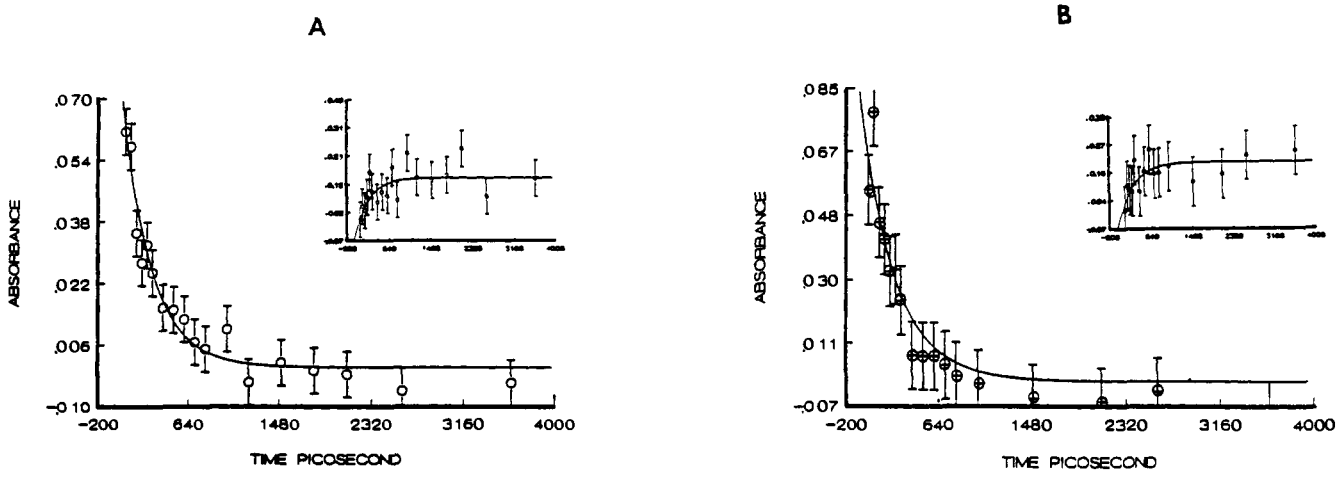

Figure 4. Picosecond decay of (A) N^+ and (B) C^+ by first-order kinetics (smooth curve) with k_{obsd} = 3.6 and 3.1 × 10^9 s^{-1}, respectively, following the 532-nm excitation of 0.05 M arene and 0.05 M TNO_2 in dichloromethane. The inset shows the growth of the covalent adduct (λ 550 nm) fitted to first-order kinetics (smooth curve) with the same value of k_{obsd}.

mental data with k_{obsd} = 3.6 × 10^9 and 3.1 × 10^9 s^{-1} for N^+ and C^+, respectively. [The reliability (noise) of the absorbance is shown in Figure 4 as ΔAbs = ±0.003.] The same first-order rate constants were evaluated when the absorbances were monitored at either 750 or 740 nm. Furthermore, the insets to Figure 4 show that the concomitant growth of the covalent adducts NT and CT occurred with the same first-order kinetics (Table III), despite the larger scatter of the experimental data arising from the relatively low absorbances of the 550-nm bands (see insets to Figure 1).

The related formyl derivative F^+ decayed with a slightly slower first-order rate constant of k_{obsd} = 2.8 × 10^{-9} s^{-1} under the same conditions. However, with this cation, the absorbance did not return completely to the base line within the time span of 2.6 ns, but it leveled off at a small residual value of Abs = 0.04. [The extent to which the cation absorbance failed to return to the base line within the alloted time span of 2.6 ns is designated hereafter as the residual fraction $R = Abs_{2.5\ ns}/Abs_{0\ ns}$, i.e., R = 0 for N^+ and C^+, and R = 0.25 for F^+.] It is also noteworthy that the first-order rate constant for the decay of F^+ accounted for only the initial fraction of the covalent adduct FT (see the Experimental Section).

The decay behavior of the cations derived from anthracene (H^+), methylanthracene (M^+), and vinylanthracene (V^+) differed in two ways from their more electron-poor analogues N^+, C^+, and F^+ presented above. First, the first-order rate constants k_{obsd} were significantly slower, and they decreased in the order $N^+ > C^+ > F^+ > H^+ > V^+ > M^+$, as listed in Table III. More important is the rather pronounced change in the decay profile illustrated in Figure 5, which reveals the leveling off of the cation absorbances at relatively high residual fractions of R = 0.75, 0.60, and 0.48 for M^+, V^+, and H^+, respectively.

III. **Solvent Effects on the Patterns of Cation Decay.** When the anthracene cation (H^+) was generated in acetonitrile solution by the 532-nm excitation of the EDA complex [H,TNO_2], the

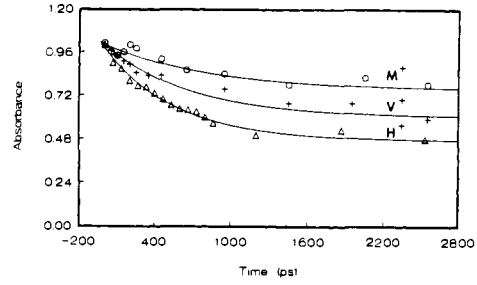

Figure 5. Pronounced differences in the residual fractions (R) found in the spectral decays of the cations H^+ (hydrogen), V^+ (vinyl), and M^+ (methyl) in dichloromethane.

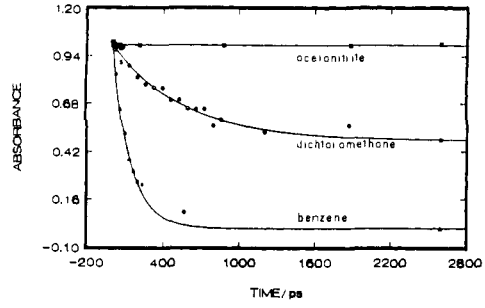

Figure 6. Solvent-induced variation of the decay profiles of the cation H^+ accompanying the changes in the residual fraction from R = 1.0 (acetonitrile) to 0.48 (dichloromethane) to 0 (benzene).

diagnostic absorption band of H^+ at λ_{max} 725 nm (Table I) persisted unchanged to beyond 2.6 ns. At the opposite extreme, the cation absorbance in benzene solution decayed rapidly to the base line, and no residual H^+ was apparent beyond 600 ps (60 ps in *n*-hexane). Figure 6 compares the striking difference in the

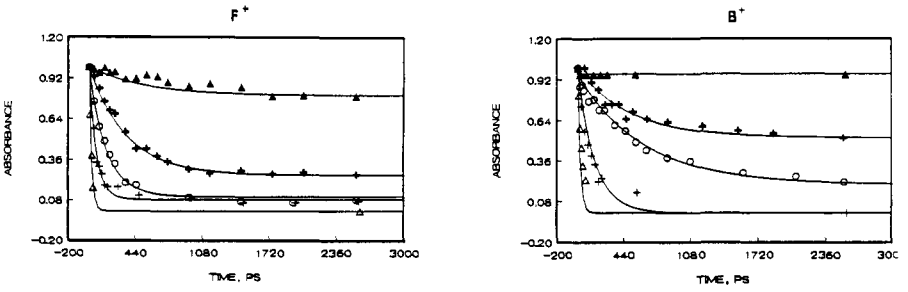

Figure 7. Graphical fit of the picosecond decays to first-order kinetics (smooth curves) in *n*-hexane (△), benzene (+), chloroform (○), dichloromethane (✚), and acetonitrile (▲) to illustrate the differing kinetic behavior of F^+ (left) and B^+ (right).

Table IV. Solvent Effect on the Picosecond Rates and Residuals for Cation Decay[a]

	MeCN		CH_2Cl_2		$CHCl_3$		C_6H_6		*n*-C_6H_{14}	
cation	k_{obsd}	*R*	k_{obsd}	*R*	k_{obsd}	*R*	k_{obsd}	*R*	k_{obsd}	*R*
N^+	1.0	0.50	3.6	0	4.4	0.13	30	0	*b*	*b*
C^+	1.5	0.50	3.1	0	5.6	0	30	0	*b*	*b*
F^+	2.0	0.80	2.8	0.25	5.4	0.10	14	0.02	>40	0
H^+	*c*	1.0	1.8	0.48	1.1	0.18	7.1	0	>40	0
B^+	*c*	1.0	1.6	0.50	1.7	0.20	6.1	0	19	0
V^+	*c*	1.0	1.5	0.60	1.0	0.75	1.5	0.05	31	0
M^+	1.0	0.56[d]	1.2	0.75	1.0	0.70	2.0	0	33	0

[a] First-order rate constants (k_{obsd}) at 23 °C in units of 10^9 s^{-1} and the residual fractions (*R*), as defined in the text. [b] Not examined. [c] Unmeasurable. [d] See the Experimental Section.

decay profiles of H^+ in acetonitrile, dichloromethane, and benzene to represent solvents of decreasing polar character, as indicated by the trend in their dielectric constants of D = 37.5, 9.1, and 2.3, respectively.[40]

The same solvent effect on the decay patterns was generally observed for all of the cations included in Table I. For example, Figure 7 compares the specific behavior of the relatively reactive cation F^+ with a less reactive one (B^+) in the most polar solvent (acetonitrile), in which the residual fraction *R* increases from 0.8 to 1.0. The smooth (decay) curves in Figure 7 were first-order plots fitted to the picosecond absorbances by the nonlinear least-squares method presented above. The kinetic differences were more apparent in solvents of intermediate polarity, such as dichloromethane, in which the first-order rate constant for F^+ decreased from $k_{obsd} = 2.8 \times 10^9$ s^{-1} to 1.6×10^9 s^{-1} for B^+, as *R* increased from 0.25 to 0.50. The largest first-order rate constants were observed in the least polar solvents benzene and *n*-hexane.

The solvent effects on all of the cation decays are collected in Table IV with respect to the values of both k_{obsd} and *R*. The results in Table IV show that the solvent effect on the decay rate consistently parallels the substituent effect. Thus the magnitude of k_{obsd} was the smallest in the most polar solvent (acetonitrile) and for the cation with the best donor substituent (Y = methyl); likewise, k_{obsd} was the largest in the least polar solvent (*n*-hexane) and for the cation with the worst donor substituent (Y = nitro). Such trends in the rate constant were reversed in the residual fraction—*R* generally was the smallest in *n*-hexane and for Y = nitro.

IV. Quantitative Salt Effects on the Kinetics of Cation Decay. The influence of salt on the cation decays was examined in the presence of the tetra-*n*-butylammonium cation (TBA^+) paired with the innocuous anion perchlorate (= P^-) and the common anion trinitromethide (= T^-) to represent the distinctive salts TBA^+P^- and TBA^+T^-, respectively. The presence of 0.1 M solutions of either TBA^+P^- or TBA^+T^- had no effect on the temporal behavior of H^+ in the most polar solvent acetonitrile, with the cation persisting without any sign of decay up to 2.5 ns in the manner described in Table IV without added salt. The same result was observed for the cation decays in the least polar solvent benzene (TBA$^+$P$^-$ was insoluble in *n*-hexane).

Table V. Effect of Salt Concentration on Cation Decay[a]

added salt[b] (mM)	k_{obsd}[c] (10^9 s^{-1})	*R*
0	1.8 (1.8)	0.48 (0.48)
2	2.1 (1.6)	0.50 (0.51)
5	1.6 (2.0)	0.52 (0.53)
10	1.4 (2.2)	0.54 (0.53)
20	1.4 (1.8)	0.58 (0.55)
30	2.1 (*d*)	0.62 (0.56)
40	2.2 (*d*)	0.64 (0.59)
50	1.6 (*d*)	0.62 (0.62)
100	1.7 (1.6)	0.64 (0.62)

[a] For the cation H^+ in dichloromethane as given in Table III. [b] TBA^+P^- and TBA^+T^-. [c] First-order rate constant for cation decay measured in the presence of TBA^+P^-(TBA^+T^-). [d] Not measured.

Table VI. Variation of the Salt Effect with Cation Structure in Different Solvents[a]

	MeCN		CH_2Cl_2		$CHCl_3$		C_6H_6[b]	
cation	k_{obsd}	*R*	k_{obsd}	*R*	k_{obsd}	*R*	k_{obsd}	*R*
N^+	2.0	0.65	3.6	0.10	*c*	*c*	*c*	*c*
C^+	2.0	0.60	3.1	0.10	*c*	*c*	*c*	*c*
F^+	2.1	0.82	3.3	0.50	5.0	0.20	14	0.10
B^+	*d*	1.0	1.6	0.65	2.4	0.37	6.2	0
H^+	*d*	1.0	2.0	0.64[e]	1.4	0.47	6.9	0
V^+	*d*	1.0	1.0	0.80	1.0	0.90	1.6	0.10
M^+	*c*	*c*	2.0	0.80	1.5	0.80	*c*	*c*

[a] First-order rate constants (k_{obsd}) at 23 °C in units of 10^9 s^{-1} under the conditions in Table IV but with 0.10 M TBA^+P^- as added salt, except as indicated otherwise. [b] Saturated solution of TBA^+P^- ($\sim 10^{-2}$ M). [c] Not examined. [d] Unmeasurable. [e] R = 0.57 with $TBA^+PF_6^-$ as the added salt.

In marked contrast to the unexceptional salt effect on the decay of H^+ in acetonitrile and benzene, the presence of TBA^+P^- and TBA^+T^- in solvents of intermediate polarity (dichloromethane and chloroform) altered both the rate (k_{obsd}) as well as the residual fraction (*R*) in measure with the salt concentration, as listed in Table V.

The salt effect was also examined with different cations by measuring the rates (k_{obsd}) and residuals (*R*) with standard amounts of added TBA^+P^- in various solvents. The results in Table VI show the salt effect on all cations to always be most pronounced in dichloromethane and chloroform, particularly with respect to increased values of *R*.

Discussion

The appearance of the transient absorption spectra of the cations Ar^+ in Figures 1–3 and Table I relates to their spontaneous generation on the picosecond time scale.[22] Importantly, the subsequent temporal evolution of the contact ion pairs as [Ar^+,T^-] can be reliably measured by focusing on the cation absorbances, since the equimolar concentration of the transients [Ar^+] = [T^-] is established in this system.[27]

For the series of structurally related contact ion pairs (CIP) pertinent to Table III, the substituent Y modulates the cation reactivity in measure with the values of $E_{ox}°$ (Table III)[31] that parallel the Hammett σ (substituent) constants.[41] As such, N^+

(40) Maryott, A. A.; Smith, E. R. *Table of Dielectric Constants of Pure Liquids*; NBS Circular 514; NBS: Washington, D.C., 1951.

Table VII. Microdynamical Rate Constants for Internal Return and Solvent Separation[a]

	MeCN		CH_2Cl_2		$CHCl_3$		C_6H_6		n-C_6H_{14}	
cation	k_1	k_2	k_1	k_2	k_1	k_2	k_1	k_2	k_1	k_2
N^+	0.5	0.5	3.6	c	3.8	0.6	30	c	b	
C^+	0.7	0.7	3.1	c	5.6	c	30	c	b	
F^+	0.4	1.6	2.1	0.7	4.9	0.5	14	0.2	>40	c
H^+	c		0.90	0.9	0.7	0.2	7.1	c	>40	c
B^+	c		0.80	0.8	1.4	0.3	6.1	c	19	c
V^+	c		0.60	0.9	0.25	0.75	1.4	0.06	31	c
M^+	0.4[d]	0.6[d]	0.30	0.9	0.30	0.7	2.0	c	33	c

[a] From the data in Table IV as described in the text. Rate constants in 10^9 s^{-1} (±10%). [b] Not examined. [c] Unmeasurable. [d] See the Experimental Section.

(Y = nitro) and M^+ (Y = methyl) represent the opposite extremes of cation reactivity[42]—they have the most and the least electrophilic character, respectively, toward the counteranion T^-.

I. Microdynamical Rate Constants for Internal Return of CIP. The annihilation of the contact ion pair is shown by the first-order disappearance of N^+ and C^+, and the complete absorbance drop to the spectral base line in Figure 4 represents the exclusive formation of the covalent adducts NT and CT (Table II). Accordingly, in the context of the Winstein formulation in Scheme I, the measured first-order rate constant defines complete (100%) internal return, that is,

$$ArT \xleftarrow{k_1} [Ar^+,T^-] \tag{6}$$

for the most electrophilic cations $Ar^+ = N^+$ and C^+ in dichloromethane. The intrinsically least reactive cations M^+ (methyl) and H^+ (hydrogen) suffer complete internal return only in the least polar hydrocarbon media, as indicated in Table IV by the absence of the residual (R) in benzene. Thus when $R = 0$, the experimental first-order rate constant $k_{obsd} = k_1$, i.e., the microdynamical rate constant for internal return in eq 6. The change in the medium from dichloromethane to benzene reflects a decrease in solvent polarity,[9] and the results in Table IV show that R generally decreases in the order acetonitrile > dichloromethane > chloroform > benzene.

II. Microdynamical Rate Constants for Internal Return of CIP versus Solvent Separation to SSIP. The nonzero values of the residual (R) obviously relate to the presence of additional pathways for cation behavior that do not lead to ion-pair annihilation (i.e., internal return). Indeed, the opposed trend of the residuals listed in Table IV to (a) decrease with solvent polarity (MeCN ≫ C_6H_6) and (b) increase with cation stability ($M^+ > N^+$) accords with Winstein's formulation of CIP behavior in its ready conversion into the solvent-separated ion pair (SSIP),

Scheme II

$$ArT \xleftarrow{k_1} [Ar^+,T^-] \xrightarrow{k_2} Ar^+//T^- \tag{7}$$

for which the residual fraction is readily given as

$$R = k_2/(k_1 + k_2) \tag{8}$$

Since the absorption spectra of the anthracene cations are unaffected by ion pairing with T^-,[34] it follows that the cation absorbance $(Abs)_t$ at a given time (t) represents the composite of the CIP and SSIP contributions:[43]

$$(Abs)_t = \exp[-(k_1 + k_2)t] + k_2(k_1 + k_2)^{-1}\{1 - \exp[-(k_1 + k_2)t]\} \tag{9}$$

$$= \frac{k_2}{k_1 + k_2} + \frac{k_1}{k_1 + k_2}\exp[-(k_1 + k_2)t] \tag{10}$$

(41) Exner, O. *Correlation Analysis in Chemistry*; Chapman, N. B., Shorter, J., Eds.; Plenum: New York, 1978; p 455. Of the various substituent constants available, the best correlations are obtained with sigma (para), and they are designated throughout this report as σ.

(42) For the substituent effect on cation reactivities, see: Ritchie, C. D. *Can. J. Chem.* **1986**, *64*, 2239.

Table VIII. Ion-Pair Reversibility of CIP and SSIP

cation[a]	k_2 (s^{-1})	k_{-2}[b] (s^{-1})	K_{IP} (k_{-2}/k_2)	ΔG_{IP} (kcal mol^{-1})
H^+	9.0×10^8	4.3×10^7	0.048	1.8
B^+	1.2×10^9	4.6×10^7	0.038	1.9
V^+	9.0×10^9	2.1×10^7	0.023	2.2

[a] Paired with T^- as given in Table III. [b] From ref 27a.

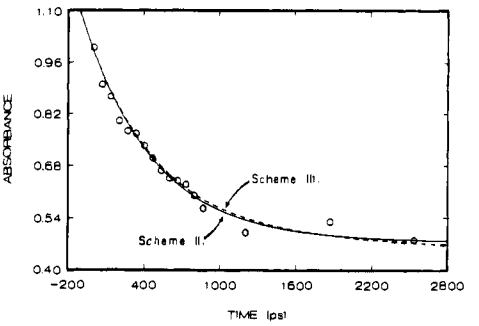

Figure 8. Effect of external return (k_{-2}) from SSIP on the picosecond decay of H^+ in dichloromethane according to Scheme III (---) in comparison with that predicted from Scheme II (—).

When $k_1 \approx k_2$, the initial first-order decay corresponds to the experimental rate constant

$$k_{obsd} = k_1 + k_2 \tag{11}$$

and eq 10 predicts the limiting value of the absorbance change that is observed in Figure 5. The simultaneous solution of eqs 8 and 11 for the experimental observables k_{obsd} and R in Table IV yields the individual rate constants k_1 and k_2 tabulated in Table VII.

Solvent separation of the contact ion pair is evaluated in Table VII by the microdynamical rate constant k_2 in Scheme II. However, the conversion of CIP to SSIP must also be considered in the light of the microscopic reverse process in order to present a more complete formulation of ion-pair dynamics:

Scheme III

$$ArT \xleftarrow{k_1} [Ar^+,T^-] \underset{k_{-2}}{\overset{k_2}{\rightleftharpoons}} Ar^+//T^- \tag{12}$$

The importance of such an ion-pair reversibility is evaluated by the first-order rate constant k_{-2} for external ion-pair return, as previously measured in the time-resolved nanosecond studies,[27] and for convenience, they are collected in Table VIII. The absorbance change accompanying the cation decay according to Scheme III is given by[43]

$$(Abs)_t = (C_1/k_{-2})[\lambda_+ + k_1 + k_2 + k_{-2}]\exp\lambda_+ t + (C_2/k_{-2})[\lambda_- + k_1 + k_2 + k_{-2}]\exp\lambda_- t \tag{13}$$

where $\lambda_\pm = [-(k_1 + k_2 + k_{-2}) \pm \{(k_1 + k_2 + k_{-2})^2 - 4k_1k_{-2}\}^{1/2}]/2$, $C_1 = [-(k_1 + k_2) - \lambda_-](\lambda_+ - \lambda_-)^{-1}$, and $C_2 = [\lambda_+ + (k_1 + k_2)](\lambda_+ - \lambda_-)^{-1}$. Figure 8 shows a typical cation decay on the picosecond time scale based on Scheme III,[44] and the graphical comparison with that based on Scheme II clearly establishes their equivalence within the experimental uncertainties of the absorbance change. Indeed, Table VIII (column 5) shows that the negligible contribution of external return to the picosecond dynamics of ion-pair behavior arises from the endergonic free energy change of 2 kcal mol^{-1} for the (re)conversion of SSIP to CIP.

III. Solvent Effects on Ion-Pair Dynamics. The distinctive effects of solvent variation on the picosecond decays are illustrated in Figure 6 by the marked variation in the residual fraction (R). The unambiguous dissection of the experimental parameters k_{obsd} and R in Table VII provides the microdynamic rate constants k_1

(43) For the derivation, see the Appendix.

(44) With the values of k_1 and k_2 taken from Table VII and k_{-2} from Table VIII.

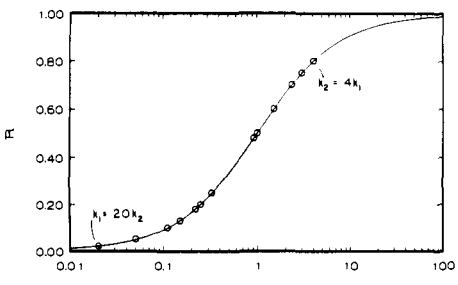

Figure 9. Interdependence of the residual fraction (R) and the microdynamical rate constants (k_2/k_1), with the circles showing the kinetics range encompassed in this study.

and k_2 for internal return and solvent separation, respectively, as described by Scheme III. The interdependence of R and the microdynamics is shown by the smooth curve in Figure 9.[45] The filled circles represent the available (20) set of independent data from which the values of k_1 and k_2 can be reliably evaluated within the limits $0.05 < R < 0.8$. Thus, in the region of the residual $R < 0.05$, only internal return can be measured since solvent separation is not competitive ($k_1 \gg k_2$).[46a] Conversely, for $R > 0.8$, internal return is too slow to provide any information about solvent separation.[46b] Thus the analysis of the picosecond dynamics accompanying CIP relaxation, as enabled by the measurement of the competition from the irreversible internal return, is limited in practice to 2 decades in relative rates, i.e., $0.1 < (k_2/k_1) < 10$, as follows.

The effect of cation structure on the internal return and solvent separation can be evaluated by the Hammett σ (substituent) parameter owing to its direct dependence on $E_{ox}°$ (vide supra). Figure 10A shows that the rate of CIP conversion to SSIP in dichloromethane is singularly insensitive to cation reactivity, i.e., $\rho_2 = 0$. By contrast, the rate of internal return of the CIP to the covalent adduct is faster for N^+ (nitro) than M^+ (methyl) by a sensitivity factor of $\rho_1 = 1.0$.

In order to consider the solvent effects on ion-pair dynamics, let us focus on the Kosower Z-value as an empirical measure of solvent polarity, since it derives specifically from the interionic stabilizations of [pyridinium,iodide] ion pairs[47]—not unlike the CIPs pertinent to this study. Thus, the solvent effect on the microdynamical rate constants k_1 and k_2 for the CIP from the prototypical cation F^+ (Table VII) is shown in Figure 10B as a function of Z. The opposed trends in the rate constants—i.e., k_2 to increase and k_1 to decrease linearly with Z—are consistently followed by the contact ion pairs derived from all of the cations in Table VII. Let us thus consider what the variation of these microdynamical rate constants with solvent polarity tells us about contact ion pairs and their dynamic behavior.

(a) For the variation of k_2 with the solvent polarity (Z), the positive slope $\zeta_2 = 0.05$ in Figure 10B is in accordance with the conversion of a "tight" CIP to a "loose" (i.e., more polar) SSIP, as originally envisaged by Winstein and co-workers.[5,6] Importantly, the constancy of k_2 irrespective of the σ (substituent) constant in Figure 10A suggests that all CIPs, independent of cation reactivity, have more or less the same (interionic) structure.[48]

(b) For the variation of k_1 with the solvent polarity (Z), the slope $\zeta_1 = -0.09$ in Figure 10B is in accordance with the annihilation of the CIP to its uncharged covalent adduct, which follows from the reactant being more polar than the activated complex. Such a trend suggests that the internal return is determined by the heterolytic strength of the new bond, i.e., the stability of the covalent adduct.[49] This conclusion is also consistent with (a) the variation of k_1 with cation reactivity (positive slope of $\rho_1 = 1.0$ in Figure 10A) as an indication of electron availability in the new bond and (b) the invariant structure of the contact ion pair (vide supra).

Table IX. Solvent Effects on the Competition between Solvent Separation and Internal Return of CIP

contact ion pair	substituent σ^a	substituent $k_1{}^b$	solvent $\zeta_1{}^c$	crossing point $Z_{iso}{}^d$
N^+T^-	0.81	3.6	−0.10	69.9
C^+T^-	0.71	3.1	−0.09	70.6
F^+T^-	0.47	2.1	−0.09	69.4
B^+T^-	0.26	0.80	−0.08	67.8
H^+T^-	0	0.90	−0.12	66.0
V^+T^-	−0.01	0.60	−0.12	64.0
M^+T^-	−0.14	0.30	−0.14	63.5

[a] Hammett substituent constant from ref 41. [b] Internal return in dichloromethane. [c] Slope of the k_1 variation (±20%) at $k_1 = k_2$, as defined in the text. [d] See text.

IV. Relevance of the Picosecond Dynamics of CIP to Solvolysis Kinetics. The clear delineation of the microdynamical rate constants k_1 and k_2 allows the efficiency of ion production from the contact ion pair to be quantitatively evaluated—especially as it is modulated by solvent polarity and cation reactivity (substituent). For example, the opposed trends in k_1 and k_2, as typically presented in Figure 10B, always lead to a crossing point Z_{iso} at which $k_1 = k_2$. Since every cation shows the same general trend of k_1 with Z and k_2 is independent of the substituent, all of the plots are characterized by a crossing point that varies monotonically with cation reactivity (Table IX). The more or less linear trend in Z_{iso} with σ as shown in Figure 11 relates to the effect of solvent polarity on the efficiency for SSIP production (relative to internal return) for cations of various electrophilic reactivity. Thus a reactive cation such as N^+ (nitro) requires a more polar solvent (Z_2) by an amount $Z_2 - Z_1 = 6.5$ kcal mol^{-1} to achieve the same degree of ionic efficiency as the solvent (Z_1) used for M^+ (methyl) under a given set of conditions. Since the microscopic reverse is applicable to solvolysis, it follows that Z_{iso} can be used to evaluate the solvent efficiency for bond heterolysis of an alkyl derivative R–X in order to optimize the additional reactions[6] that proceed from the solvent-separated ion pair $R^+//X^-$ in Scheme I.

V. Salt Effects on the Picosecond Dynamics of Contact Ion Pairs. The effect of added salt on the picosecond dynamics of CIP is largely manifested (Tables V and VI) by changes in the residual fraction (R) without significantly altering the kinetics (k_{obsd}). Accordingly, the dynamics in Scheme III is modified by the inclusion of ion exchange (k_x) as shown in Scheme IV:

Scheme IV

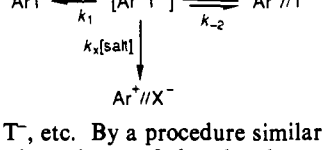

where $X^- = P^-$, T^-, etc. By a procedure similar to that used in eq 10, the time dependence of the absorbance change in the presence of added salt is[43]

$$(\mathrm{Abs})_t = \frac{k_2 + k_x[\mathrm{salt}]}{k_1 + k_2 + k_x[\mathrm{salt}]} + \frac{k_1}{k_1 + k_2 + k_x[\mathrm{salt}]} \exp[-(k_1 + k_2 + k_x[\mathrm{salt}])t] \quad (14)$$

(45) Based on the following relationship: $R/(1 - R) = k_2/k_1$.

(46) (a) The practical lower limit can be set at $k_1 > 20k_2$. (b) The practical upper limit is $k_2 > 4k_1$, as limited by the signal-to-noise level in the absorbance data.

(47) (a) Kosower, E. M. *J. Am. Chem. Soc.* **1958**, *80*, 3253. For a summary, see C. Reichardt in ref 9. (b) Kosower, E. M. *Physical Organic Chemistry*; Wiley: New York, 1968.

(48) The substituent (Y) is unlikely to affect both the CIP and SSIP to the same degree, unless both the cation and anion exist intact (each with unit charge and no partial binding) in both ion pairs and the interionic separation in the CIP is invariant with Y.[47b]

(49) Since the oxidation potential of trinitromethide [$E° = 1.95$ V in Kokorakina, V. A.; Foektistov, L. G.; Shevelev, S. A.; Fianzil'berg, A. A. *Elektrokhimiya* **1970**, *6*, 1849] is more positive than that of anthracene with $E° = 1.5$ V,[31a] the driving force for back electron transfer (i.e., $Ar^+,T^- \rightarrow Ar,T$) is endergonic. It is thus likely that ion-pair annihilation proceeds by the direct formation of the Ar–T bond.

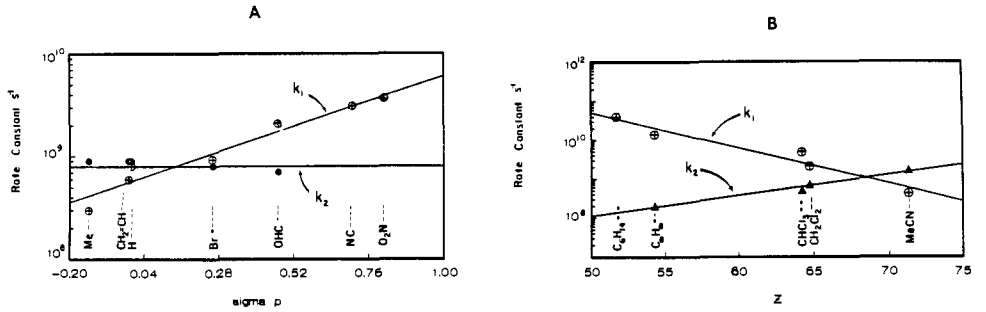

Figure 10. Effect of cation reactivity (σ) on the rate constants for internal return (k_1) and solvent separation (k_2) in dichloromethane (A), with the lines defining the slopes $\rho_1 = 1.0$ and $\rho_2 = 0$, respectively, and effect of solvent polarity (Kosower Z-value) on k_1 and k_2 for F^+ (B), with the lines defining the slopes $\zeta_1 = -0.09$ and $\zeta_2 = 0.05$, respectively.

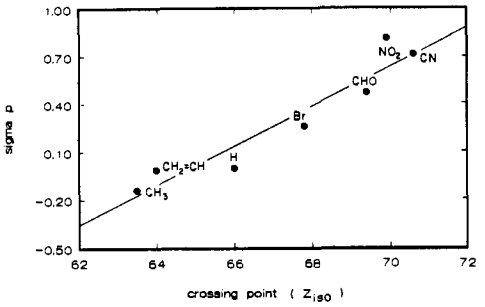

Figure 11. Solvent effect on the efficiency of ion production for cations of different electrophilic reactivity (σ) as evaluated by the variation in the solvent crossing point Z_{iso}.

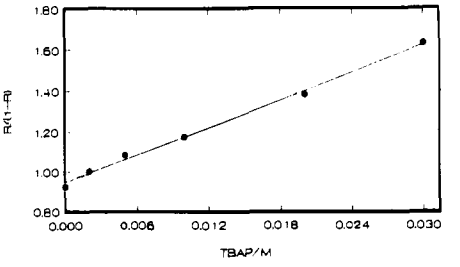

Figure 12. Ion-pair exchange of CIP with added TBA^+P^- as measured by changes in the residual fraction of H^+ in dichloromethane according to eq 17.

where k_x is the second-order rate constant for ionic exchange, for example,

$$Ar^+,T^- + TBA^+P^- \overset{k_x}{\rightleftharpoons} Ar^+//P^- + TBA^+T^- \qquad (15)$$

Since the residual fraction in eq 14 is

$$R = (k_2 + k_x[\text{salt}])/(k_1 + k_2 + k_x[\text{salt}]) \qquad (16)$$

it can be reexpressed in the more convenient form

$$\frac{R}{1-R} = \frac{k_x[\text{salt}]}{k_1} + \frac{k_2}{k_1} \qquad (17)$$

The absorbance data for H^+ up to the salt concentration of 0.03 M TBA^+P^- in Table V are plotted in Figure 12 according to eq 17, and the rate constant ratios k_x/k_1 and k_2/k_1 are provided by the slope and intercept, respectively. The values of $k_x = 2.1 \times 10^{10}$ and 9.4×10^9 M^{-1} s^{-1} for TBA^+P^- and TBA^+T^-, respectively, are based on the value of $k_1 = 9.0 \times 10^8$ s^{-1} in Table VII. The accompanying values of $k_2 = 8.8 \times 10^8$ and 9.8×10^8 s^{-1} are essentially the same as that (9×10^8 s^{-1}) obtained in the absence of salt and thus lend credence to the formulation in Scheme IV.

Since the molar effectiveness of added salt decreased monotonically at concentrations [salt] > 0.04 M (probably due to aggregation in dichloromethane[50]), we evaluated an effective concentration at [salt] = 0.10 M for TBA^+P^- in order to interpret the results in Table VIII. Thus with the aid of eq 17 and $k_x = 2.1 \times 10^{10}$ M^{-1} s^{-1} (vide supra), together with the parameters ($k_{obsd} = 2.0 \times 10^9$ s^{-1} and $R = 0.64$) in the last entry in Table V at 0.10 M added salt, the effective concentration $[TBA^+P^-]_{eff}$ is calculated to be 0.05 M. The exchange rates evaluated for the CIPs in Table VIII all lie in range of 10^{10} M^{-1} s^{-1}, but their accuracy based on this procedure is insufficient to delineate any dependence on cation structure.[51]

Summary and Conclusions

Time-resolved spectroscopy of contact ion pairs provides the three rate constants critical to the description of the (picosecond) ion-pair microdynamics in Scheme I, viz., those for internal return (k_1) to the covalent precursor, interionic relaxation (k_2) to the solvent-separated ion pair, and ion exchange (k_x) for the special salt effect. Indeed, the measurement of the rate constants k_1, k_2, and k_x in Table VII and Figure 12 that are applicable to the contact ion pair $[Ar^+,T^-]$ presents the quantitative basis for evaluating the initial stages of solvolysis mechanisms—insofar as the covalent adduct ArT serves the prototypal role.[52] As such, the changes in k_1 and k_2 with different Y-substituted cations (Figure 10A) and various solvents (Figure 10B) are particularly informative. In particular, the constancy of the rate of CIP relaxation to SSIP irrespective of the Y-substituent, as shown by the invariance of k_2 in Figure 10A, points to an interionic separation that does not change with cation reactivity. In other words, a single structure (dipolar with unit charges) is applicable to all contact ion pairs.[48] If so, the increasing rates of internal return with electron-poor (Y) substituents—shown by the positive slope $\rho_1 = 1.0$ for k_1 in Figure 10B—are driven by increasing stabilities of the covalent adduct. Applied to solvolysis mechanisms, this conclusion indicates that the variation in ionization rates is diametrically opposed to internal return, but both derive more from changes in stability of the reactant than of the contact ion pair—from similarly constituted derivatives (such as the aralkyl series amenable to the Hammett treatment).[52,53]

The increasing rate of CIP separation to SSIP with solvent polarity—shown by the positive slope $\zeta_2 = 0.05$ for F^+ in Figure

(50) See, for example: Goodson, B. E.; Schuster, G. B. *J. Am. Chem. Soc.* **1984**, *106*, 7254.

(51) We hope that further studies in progress will provide more extensive data on ion-pair exchange rates.

(52) The covalent adduct ArT is formally related to the ubiquitous aralkyl derivatives such as benzhydryl esters (the solvolysis kinetics of which have been studied extensively). Thus recent thermochemical measurements indicate that paramagnetic species such as the adduct ArT are equivalent to the corresponding diamagnetic species—both being dominated by their uncharged, neutral character (E. M. Arnett, presented at the Kimbrough International Symposium in the Loker Hydrocarbon Research Institute, Los Angeles, CA, January 31, 1992). Moreover, T^- is a viable, hard leaving group owing to the strong acid character ($pK_a = 0.2$) of nitroform [Dean, J. A. *Lange's Handbook of Chemistry*, 13th ed.; McGraw-Hill: New York, 1985; p 5–59] and its relatively high oxidation potential (vide supra).[49]

(53) For some recent theoretical calculations of solvolytic ion pairs and ion-pair dynamics, see: (a) Jorgensen, W. L.; Buchner, J. K.; Huston, S. E.; Rossky, P. J. *J. Am. Chem. Soc.* **1987**, *109*, 1891. (b) Keirstead, W. P.; Wilson, K. R.; Hynes, J. T. *J. Chem. Phys.* **1991**, *95*, 5256. (c) Kim, H. J.; Hynes, J. T. *J. Am. Chem. Soc.*, submitted for publication. For a theoretical calculation of the ion-pair dynamics, see ref 54.

(54) (a) Ciccotti, G.; Ferrario, M.; Hynes, J. T.; Kapral, R. *J. Chem. Phys.* **1990**, *93*, 7137. (b) Karim, O. A.; McCammon, J. A. *Chem. Phys. Lett.* **1986**, *132*, 219; *J. Am. Chem. Soc.* **1986**, *108*, 1762. (c) Hynes, J. T. *Theory of Chemical Reaction Dynamics*; Baer, M., Ed.; CRC Press: Boca Raton, FL, 1985; Vol. 4.

10B—is in accordance with the increased dipolar character of SSIP as a result of solvent intervention.[9,47] Moreover, the fit of the k_2 data in Table VII for all other cations to the same line is consistent with a single CIP structure (vide supra). Consequently, the decreasing rates of internal return with solvent polarity—shown by the opposed negative slopes ζ_1 (Table IX) that are more or less independent of cation reactivity—relate to decreasing driving forces for CIP annihilation to form the uncharged covalent adduct. Applied to solvolysis mechanisms, this conclusion strongly points to the dominant reactant stabilization (as opposed to CIP change) in structurally modulating the rates of ionization (and internal return).

The effect of added salt on the picosecond dynamics [to increase the residuals (R) monotonically in Table V] provides unambiguous evidence for the interception of the contact ion pair. Ion-pair exchange as presented in eq 15 is the most direct formulation of the linear plot in Figure 12. The special salt effect,[7] as given by the CIP lifetime of $1/k_x[\text{salt}] \approx 10$ ns at salt concentrations as low as 5×10^{-3} M, can compete effectively with internal return and solvent separation. As such, it represents experimental support for the viability of Sneen's formulation of ion-pair exchange in the contact ion pair.[7b]

Experimental Section

Materials. Anthracene (Aldrich, gold label) was used as received, and its derivatives with 9-bromo, -vinyl, -formyl, -cyano, -nitro, and -methyl substituents also obtained from Aldrich were recrystallized from ethanol prior to use. Tetranitromethane and nitroform were prepared by literature procedures.[55] Tetra-*n*-butylammonium perchlorate (G. F. Smith Co.) and tetra-*n*-butylammonium hexafluorophosphate (Aldrich) were recrystallized from ethyl acetate and dried in vacuo. Tetra-*n*-butylammonium trinitromethide was prepared from nitroform, as described previously.[56]

Acetonitrile (Baker reagent grade) was stirred with crystalline $KMnO_4$ for 1 day, and the mixture was refluxed until colorless. After the removal of MnO_2 by filtration, the acetonitrile was first distilled from P_2O_5 under an argon atmosphere. It was then fractionated from CaH_2 and stored in a Schlenk flask under an argon atmosphere. Dichloromethane (Mallinckrodt reagent) was stirred with concentrated H_2SO_4 for 4 days, during which the spent H_2SO_4 (yellow) was repeatedly replaced until it remained colorless. Dichloromethane was washed with aqueous $NaHCO_3$ and water and then dried over $CaCl_2$ and distilled from P_2O_5 under an argon atmosphere. Chloroform (Mallinckrodt reagent grade) was similarly purified with the aid of H_2SO_4, and it was stored in a Schlenk flask under an argon atmosphere as described above. *n*-Hexane (Mallinckrodt reagent) was stirred with concentrated H_2SO_4 for 1 day and then washed with aqueous $NaHCO_3$ and water. After drying with $CaCl_2$, *n*-hexane was distilled from P_2O_5 under an argon atmosphere. Benzene (Baker reagent grade) was also purified in the same manner, and it was stored in a Schlenk flask under an argon atmosphere prior to use.

Instrumentation. The UV–vis absorption spectra of the ground-state EDA complexes were measured on a Hewlett-Packard 8450A diode array spectrometer. The time-resolved differential absorption spectra on the picosecond time scale were obtained with a laser flash system that utilized the 532- (second harmonic) and 355-nm (third harmonic) 20-ps pulses from a Quantel YG501-C mode-locked Nd:YAG laser as the excitation sources. The excitation beam was focused onto the sample with a cylindrical (fused silica) lens (f 2). The white light continuum probe light (400–800 nm) was generated by focusing the 1064-nm pulse onto a 10-cm cell which contained a 1:1 (v/v) mixture of H_2O and D_2O. The white light continuum was focused onto a bifurcated fiber optic bundle (Dolan Jenner) which directed the two analyzing beams through the excited and unexcited volumes of the sample at a 90° angle to the excitation beam. The analyzing beam passed through the sample and was collected by a fiber optic cable that was connected to a monochromator (ISA HR320). The signal was recorded on a dual diode array (Princeton Instruments DD512) equipped with a OSMA controller (Princeton Instruments ST120); it was calibrated with the 436- and 542-nm lines from a mercury lamp. Time resolution was achieved by passing the 1064-nm fundamental along a delay stage (Velmex B4036Q13) to vary the path-length of the probe light with respect to the excitation beam.

Measurements of Transient Absorption Spectra and Spectral Decays. The picosecond transient absorption measurements were carried out by the 532-nm laser excitation (2 mJ per pulse) of the EDA complexes from 0.10 M aromatic donor and 0.10 M TNO_2 dissolved in the selected solvent. The transient absorption spectra were processed (with the aid of the OSMA program) by subtracting the dark spectrum from the test spectrum in order to obtain the transients uninfluenced by power fluctuations for over 300 accumulations. The maximum of the transient absorbance was set as zero time for each experiment.

Nonlinear least-squares fittings of the picosecond decays were performed with the aid of the ASYST 2.0 software based on the Gauss–Newton algorithm[39] and running on an AT&T (6300 plus) microcomputer. The curve-fitting analysis involved the following time-dependent function: $F(t) = C_1 \exp(-C_2 t) + C_3$, where C_1, C_2, and C_3 represent free-floating parameters. Optimization was carried out until C_1, C_2, and C_3 obtained from different (arbitrarily chosen) starting values were the same. After the best fit to the kinetic data was achieved, the decay was normalized: $F(t) = (C_1 + C_3)[C_1/(C_1 + C_3)] \exp(-C_2 t) + C_3/(C_1 + C_3) = (C_1 + C_3)\{[1 - C_3/(C_1 + C_3)] \exp(-C_2 t) + C_3/(C_1 + C_3)\}$. For the experimental form of the absorbance change in eq 10, i.e., $(\text{Abs})_t = (1 - R) \exp(-k_{obsd} t) + R$, where $k_{obsd} = C_2$, $R = C_3/(C_1 + C_3)$ and $C_1 + C_3 = (\text{Abs})_0$, the absorbance maximum at $t = 0$.

Figure 7 illustrates the typical fittings of eq 10 to the spectral decays of F^+ and B^+ in various solvents. Similarly, the simultaneous decays of C^+ and N^+ at λ_{max} (Table I) and the growths of their covalent adducts at $\lambda \approx 550$ nm (as shown in Figure 4) were evaluated with the same rate constant k_{obsd} listed in Table IV. The related formyl derivative F^+ decayed to $R = 0.25$, and the growth of FT was consistent with k_{obsd} (Table IV) to approximately 50% of the temporal evolution. Absorbance deviations at $t > 1$ ns were better fit with an additional exponential. The temporal evolution of the absorbances of the covalent adduct, Abs(ArT), allowed the extinction coefficients at the times listed in Table II to be evaluated from the accompanying temporal absorbances of the cation, $\text{Abs}(Ar^+)$, and its extinction coefficient $\epsilon(Ar^+)$ listed in footnote 35 by the expression $\epsilon[\text{ArT}] = \epsilon(Ar^+)[\text{Abs}(\text{ArT})]/[(\text{Abs})_0 - \text{Abs}(Ar^+)]$, where $(\text{Abs})_0$ is the cation absorbance at $t = 0$. The graphical fit of the spectral decay for the most stable cation M^+ (methyl) in the most polar solvent acetonitrile is included in Table IV (last entry, colums 2 and 3). The value of the residual fraction $R = 0.56$ is anomalously low, and it probably relates to the incursion of another decay process such as the side chain substitution presented earlier.[27] Thus the rate constants in Table VII (last entry, columns 2 and 3) include deprotonation of the methyl group in M^+.

The solvent effects on k_{obsd} and R for F^+ as listed in Table IV (entry 3) were also examined in mixtures consisting of benzene/acetonitrile and dichloromethane/acetonitrile. Thus serial experiments were carried out with benzene (2.8 mL) with the following amounts of acetonitrile (mL) and values of k_{obsd} (10^9 s^{-1}): 0, 14; 0.04, 9.4; 0.07, 7.5; 0.10, 7.4; 0.15, 4.7; 0.20, 4.8; 0.30, 3.8; 0.60, 1.4 ($R = 0$ for all). Experiments were also carried out for dichloromethane (2.80 mL) with the following amounts of acetonitrile (mL) and values of k_{obsd} (10^9 s^{-1}) and R: 0, 2.8, 0.25; 0.05, 2.8, 0.25; 0.10, 2.2, 0.25; 0.15, 2.0, 0.25; 0.20, 2.0, 0.27; 0.30, 2.0, 0.32; 0.40, 2.0, 0.36; 0.50, 2.0, 0.38; 1.00, 2.0, 0.55; 1.50, 2.0, 0.60; 2.00, 2.0, 0.60; 2.90, 2.0, 0.65 [pure CH_3CN, 2.0×10^9 s^{-1}, $R = 0.80$].

Acknowledgment. We thank the National Science Foundation and the R. A. Welch Foundation for financial support.

Appendix

Derivations of the Time-Dependent Absorbance Changes Accompanying the Cation Decays. For Scheme II, the absorption spectra of the CIP Ar^+,T^- and the SSIP $Ar^+//T^-$ are taken to be the same, and at $t = 0$, $[Ar^+,T^-] = 1$ and $[Ar^+//T^-] = [\text{ArT}] = 0$. The differential equations governing this system are as follows: $dx/dt = -(k_1 + k_2)x$, $dy/dt = k_2 y$, and $dz/dt = k_1 z$, where x, y, and z are the concentrations of CIP, SSIP, and covalent adduct, respectively. Integration yields the time dependency of CIP as $[Ar^+,T^-] = \exp[-(k_1 + k_2)t]$ and of SSIP as $[Ar^+//T^-] = k_2(k_1 + k_2)^{-1}[1 - \exp[-(k_1 + k_2)t]]$. Therefore the time-dependent change in the cation absorbance given as the sum of $[Ar^+,T^-]$ and $[Ar^+//T^-]$ is eq 10. Similarly, the time-dependent change in the adduct absorbance is $(\text{Abs})_t = k_1(k_1 + k_2)^{-1}[1 - \exp[-(k_1 + k_2)t]]$.

For Scheme III, the pertinent rate expressions are the following:

$$\frac{d[Ar^+,T^-]}{dt} = -(k_1 + k_2)[Ar^+,T^-] + k_2[Ar^+//T^-] \quad (18)$$

$$\frac{d[Ar^+//T^-]}{dt} = k_2[Ar^+,T^-] - k_{-2}[Ar^+//T^-] \quad (19)$$

(55) Liang, P. *Organic Syntheses*; Wiley: New York, 1955; Collect. Vol. III, p 803.
(56) Homer, J.; Huck, P. J. *J. Chem. Soc. A* **1968**, *277*.

The solutions to the differential eqs 18 and 19 are

$$[Ar^+,T^-] = C_1 \exp(\lambda_+ t) + C_2 \exp(\lambda_- t) \quad (20)$$

$$[Ar^+//T^-] = (C_1/k_{-2})[\lambda_+ + k_1 + k_2] \exp(\lambda_+ t) + (C_2/k_{-2})[\lambda_- + k_1 + k_2] \exp(\lambda_- t) \quad (21)$$

where C_1, C_2, λ_+, and λ_- are the rate constant terms given in the text (with eq 13). Since $(Abs)_t = [Ar^+,T^-] + [Ar^+//T^-]$, the time-dependent absorbance change is given in eq 13.

For Scheme IV, the effect of salt is included in the rate expression as

$$\frac{d[Ar^+,T^-]}{dt} = -(k_1 + k_2 + k_x[salt])[Ar^+,T^-] \quad (22)$$

$$\frac{d[Ar^+//X^-]}{dt} = k_x[salt][Ar^+,T^-] \quad (23)$$

in addition to the k_1 and k_2 terms given above. [The reverse of eq 15 is neglected since the SSIP is more stable than the CIP and $[TBA^+P^-] \gg [TBA^+T^-]$]. Integration gives the time-dependent variation in concentration as

$$[Ar^+,T^-] = \exp[-(k_1 + k_2 + k_x[salt])t] \quad (24)$$

$$[Ar^+//T^-] = k_2\{k_1 + k_2 + k_x[salt]\}^{-1}\{1 - \exp[-(k_1 + k_2 + k_x[salt])t]\} \quad (25)$$

$$[Ar^+//X^-] = k_x[salt]\{k_1 + k_2 + k_x[salt]\}^{-1}[1 - \exp\{-(k_1 + k_2 + k_x[salt])t\}] \quad (26)$$

Since $(Abs)_t = [Ar^+,T^-] + [Ar^+//T^-] + [Ar^+//X^-]$, the time-dependent absorbance change is eq 14.

Registry No. $ArNTNO_2$, 91452-21-0; $ArCTNO_2$, 91452-20-9; $ArFTNO_2$, 91452-22-1; $ArBTNO_2$, 91452-19-6; $ArHTNO_2$, 36301-08-3; $ArVTNO_2$, 96689-10-0; $ArMTNO_2$, 140225-65-6.

Chiral Molecular Recognition in Monolayers of Diastereomeric *N*-Acylamino Acid Methyl Esters at the Air/Water Interface

Jonathan G. Heath and Edward M. Arnett*

Contribution from the Gross Chemical Laboratory, Department of Chemistry, Duke University, Durham, North Carolina 27706. *Received December 23, 1991*

Abstract: This article continues our study of the effects of headgroup geometry and temperature on chiral recognition in the force–area isotherms, thermodynamics of spreading, and surface shear viscosities of monolayers and mixed monolayers of long-chain amino acid ester surfactants. *N*-Stearoyl—and lauroyl—derivatives of the methyl esters of cysteine, cystine, and threonine are compared to the previously-reported serine derivative. The structural points at issue are as follows: (a) the effects of replacing the hydroxyl group of serine with the thiol group of cysteine; (b) the effect of joining two cysteine groups through their sulfur atoms to produce the two-chain cystine surfactant; and (c) the effect of attaching a methyl group to the carbon bearing the hydroxyl group in stearoylserine methyl ester (SSME) to produce the bulkier stearoylthreonine methyl ester (STME). Comparison is first made for the melting point versus enantiomer composition of the crystals for each compound. In all four cases a racemate is formed. Next, the corresponding effects of enantiomeric composition versus the appropriate surface properties are presented and behavior similar to the melting point curves is seen, implying stereoselective behavior when the monolayers are in equilibrium with their crystals or quasicrystalline condensed surface phases. Diastereomeric effects were small, since *meso*-dilauroylcystine dimethyl ester (DLCDME) showed properties which were nearly identical to its D and L enantiomers, and the allo form of STME was similar to its enantiomers. All four compounds showed distinctly different force–area curves for their enantiomers versus their racemic mixtures, but the shapes of the curves and phase behavior (between liquid-expanded and liquid-condensed films) depended heavily on temperature. All force–area curves show hysteresis effects in the difference between the compression and expansion regions, indicating, as we have shown before, that relaxation of compressed monolayer states is slow and that the films are in metastable states. Phase behavior is an erratic function of headgroup and temperature. Also, there is no general pattern of whether racemates or enantiomers are most expanded. No crystals of quality sufficient for X-ray analysis could be grown, so rigorous interpretation of properties and behavior in terms of structure cannot be made. However, clear differences between the behavior of stearoylcysteine methyl ester (SCME) and SSME can be interpreted in terms of hydrogen bonding of the serine hydroxyl group to the water subphase. Furthermore, comparison of force–area curves for a series of diastereomeric mixtures of L-STME and L-*allo*-STME with D- and L-SSME suggests that the stereochemistry at the carbon between the ester and amide functions is primarily responsible for the stereoselectivity in the packing of STME films. Films of SCME were too condensed to allow a surface viscosity study, but those of DLCDME and STME exhibited Newtonian flow with essentially no stereoselectivity in their flow properties.

Introduction

There is a rapidly growing appreciation of the importance of intermolecular forces in determining chemical reactivity in a wide variety of systems of condensed matter, with much current interest in the "molecular recognition" factors that are responsible for the extraordinary selectivity and catalytic power of enzymes.[1-4] Stereochemistry is the most sensitive tool for probing the structural details of how molecules "see" each other as they come together to form complexes and transition states.

The elegant techniques of surface chemistry developed by Irving Langmuir and his colleagues for manipulating monolayer films at the air/water interface provide a unique means not only to measure intermolecular forces quantitatively but to control them at will. However, despite a considerable history of research which has explored the relationships between the structures of surfactants

(1) Breslow, R. *Pure Appl. Chem.* **1990**, *62*, 1859.
(2) Lehn, J.-M. *Angew. Chem., Int. Ed. Engl.* **1990**, *29*, 1304.
(3) Ikeura, Y.; Kurihara, K.; Kunitake, T. *J. Am. Chem. Soc.* **1991**, *113*, 7342.
(4) Rebek, J., Jr. *Angew. Chem., Int. Ed. Engl.* **1990**, *29*, 245.

0002-7863/92/1514-4500$03.00/0